JACS
JOURNAL OF THE AMERICAN CHEMICAL SOCIETY

ARTICLE

pubs.acs.org/JACS

Binding of Low Molecular Weight Inhibitors Promotes Large Conformational Changes in the Dengue Virus NS2B-NS3 Protease: Fold Analysis by Pseudocontact Shifts

Laura de la Cruz,[†] Thi Hoang Duong Nguyen,[†,§] Kiyoshi Ozawa,[†] James Shin,[‡] Bim Graham,[‡] Thomas Huber,[†] and Gottfried Otting*[,†]

[†]Research School of Chemistry, Australian National University, Canberra, ACT 0200, Australia

[‡]Medicinal Chemistry and Drug Action, Monash Institute of Pharmaceutical Sciences, Parkville VIC 3052, Australia

Supporting Information

ABSTRACT: The two-component dengue virus NS2B-NS3 protease (DEN NS2B-NS3pro) is an established drug target, but inhibitor design is hampered by the lack of a crystal structure of the protease in its fully active form. In solution and without inhibitors, the functionally important C-terminal segment of the NS2B cofactor is dissociated from DEN NS3pro ("open state"), necessitating a large structural change to produce the "closed state" thought to underpin activity. We analyzed the fold of DEN NS2B-NS3pro in solution with and without bound inhibitor by nuclear magnetic resonance (NMR) spectroscopy. Multiple paramagnetic lanthanide tags were attached to different sites to generate pseudocontact shifts (PCS). In the face of severe spectral overlap and broadening of many signals by conformational exchange, methods for assignment of ^{15}N-HSQC cross-peaks included selective mutation, combinatorial isotope labeling, and comparison of experimental PCSs and PCSs back-calculated for a structural model of the closed conformation built by using the structure of the related West Nile virus (WNV) protease as a template. The PCSs show that, in the presence of a positively charged low-molecular weight inhibitor, the enzyme assumes a closed state that is very similar to the closed state previously observed for the WNV protease. Therefore, a model of the protease built on the closed conformation of the WNV protease is a better template for rational drug design than available crystal structures, at least for positively charged inhibitors. To assess the open state, we created a binding site for a Gd^{3+} complex and measured paramagnetic relaxation enhancements. The results show that the specific open conformation displayed in the crystal of DEN NS2B-NS3pro is barely populated in solution. The techniques used open an avenue to the fold analysis of proteins that yield poor NMR spectra, as PCSs from multiple sites in combination with model building generate powerful information even from incompletely assigned ^{15}N-HSQC spectra.

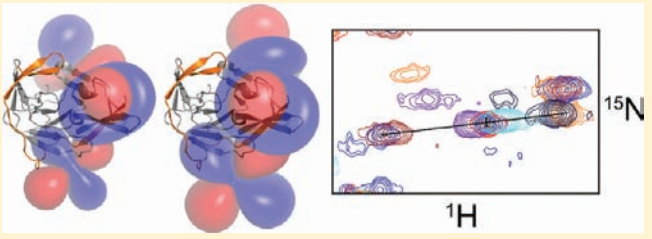

INTRODUCTION

Dengue is a considerable health hazard, putting an estimated 40% of the world population at risk especially in the tropical and subtropical regions.[1,2] During infection, the flavivirus RNA genome is translated into a polyprotein which is subsequently cleaved into several components. Viral replication depends on the nonstructural protein 3 (NS3). The N-terminal part of NS3 encodes a serine protease domain, NS3pro, which is essential for proteolysis of the polyprotein, making it a prime drug target.[3] A segment of about 40 residues from NS2B acts as a cofactor that boosts the activity of the enzyme toward peptide substrates 3300- to 7600-fold.[4] There are four dengue serotypes. Their NS2B-NS3 proteases are closely related to each other and to the corresponding protease of the West Nile virus (WNV; about 40% amino acid sequence identity). All contain the classic catalytic triad of serine proteases (His, Asp, Ser). The present article focuses on the NS2B-NS3 protease of the most studied among the dengue virus serotypes, type 2.

A 27 kDa construct, where a 47-residue segment of NS2B is fused to the N-terminus of NS3pro via a Gly_4-Ser-Gly_4 linker, retains the activity of the protease[5] and has been used for crystal structure determinations[6,7] and NMR spectroscopic studies.[8] In the following, we refer to the dengue and WNV constructs with such a covalent linkage between NS2B and NS3pro as DENpro and WNVpro, respectively. A crystal structure determined of DENpro (serotype 2) in the absence of inhibitor showed that the N-terminal part of the 47-residue NS2B segment forms an integral part of the N-terminal β-barrel of the protease,[6] but the C-terminal segment of the NS2B cofactor (NS2B-C, Glu66*-Leu95*; throughout this text, residue numbers of DEN NS2B are identified by an asterisk) was far from the active site ("open state"; Figure 1A). This was unexpected, as NS2B-C is essential for full protease activity of DENpro.[4,9−11] Remarkably, a crystal

Received: September 6, 2011
Published: October 18, 2011

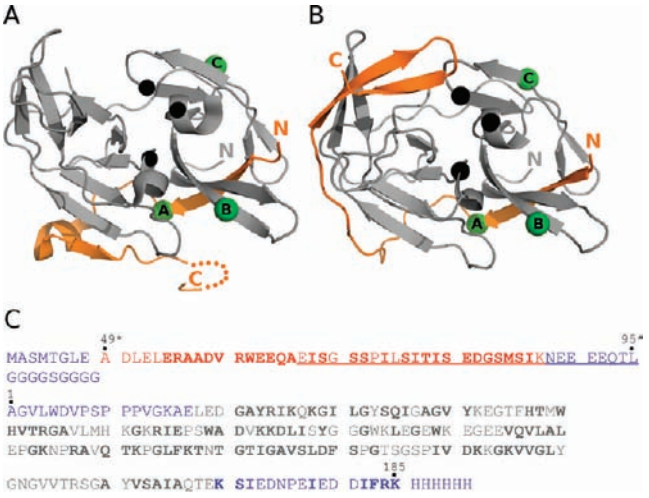

Figure 1. Structures of DEN NS2B-NS3pro, illustrating the large conformational change between open and closed conformations, and amino acid sequence. (A) Open conformation in the crystal structure (PDB accession code 2FOM[6]). NS2B is shown in orange (residues 49*−86*). NS3pro is shown in gray (residues 18−169). The C^{α} atoms of the catalytic triad in the active site are shown as black spheres. Green spheres mark the C^{α} atoms of the cysteine residues introduced by site-directed mutagenesis for subsequent labeling with lanthanide tags. The N- and C-termini of NS2B and the N-terminus of NS3pro are identified. The crystal structure is devoid of electron density for a part of NS2B (dotted line) and for 26 residues connecting the C-terminus of NS2B with the N-terminus of NS3pro. (B) Closed conformation modeled on the crystal structure of WNV NS2B-NS3pro with a peptide inhibitor (PDB accession code 2FP7[6]) as the template. The same residues are displayed as in (A). (C) Amino acid sequence of the DENpro construct used. Residues for which sequence-specific resonance assignments were obtained in the presence of inhibitor **1** are highlighted in bold. Orange and gray letters identify the segments from NS2B and NS3pro, respectively, displayed in (A) and (B). All other residues are in blue, including the N-terminal expression tag, residues 87*−95* of NS2B and 1−17 and 170−185 of NS3pro (for which crystal structures of the closed state of WNVpro display different conformations or no electron density, indicating flexibility[6,12,14]), the Gly_4-Ser-Gly_4 linker connecting NS2B with NS3pro, and the C-terminal His_6 tag. The C-terminal part of NS2B (NS2B-C) comprises residues 66*−95* (highlighted by underlining). It has been shown for WNVpro[12] that a Gly_4-Ser-Gly_4 linker between NS2B and NS3pro is compatible with the open and closed states, which can be attributed to the high mobility of the N-terminal residues of NS3pro.[16] The proline-rich N-terminal segment of DEN NS3pro is probably equally flexible.

structure of WNVpro in the absence of inhibitor was very similar.[12] Also a crystal structure of DENpro (serotype 1) showed NS2B-C far from the active site, albeit in a different location defined by crystal contacts.[7] (A crystal structure of DENpro from serotype 4 with full-length NS3 misses most of NS2B-C.[13]) In contrast, WNVpro structures determined in the presence of peptide inhibitors displayed NS2B-C in a very different conformation in which NS2B-C wraps around NS3pro and lines the substrate binding site.[6,12,14] We refer to this conformation as the "closed state" (Figure 1B). The closed conformation is thought to be the enzymatically active structure, as NS2B-C is equally essential for full protease activity in WNVpro[15] as in DENpro.[4,9−11]

Analysis of WNVpro by NMR spectroscopy established that the closed conformation is the most highly populated state in solution irrespective of the presence or absence of inhibitors but

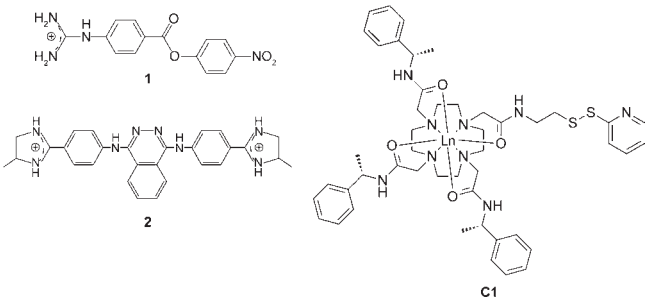

Figure 2. Chemical structures of compounds used. Throughout the text, the inhibitors are referred to as compounds **1** and **2**, respectively. **1** was first identified as a noncovalently binding inhibitor of the related protease WNVpro[34] and subsequently found to inhibit DENpro. **2** is also an inhibitor of WNVpro.[18,35] C1 and C2 were activated by a pyridin-2-yldisulfanyl group for spontaneous reaction with a cysteine thiol group to form a disulfide bond. The C2-tag is the opposite enantiomer of the C1-tag,[36] with ((*R*)-1-phenylethyl)acetamide pendants instead of ((*S*)-1-phenylethyl)acetamide pendants throughout.

that even low molecular weight inhibitors can stabilize the closed state.[16] Therefore, the open conformation of WNVpro observed by crystallography is sensitive to the crystalline environment. In contrast, NMR studies of DENpro (serotype 2) showed very narrow signals for NS2B-C,[8,17] characteristic of a highly mobile random coil polypeptide chain. In this protein, NS2B-C is thus mostly dissociated from NS3pro. The differences between the NS2B-C segments in both proteins are highlighted by the significantly lower sequence identity between the NS2B-C segments of DENpro (serotype 2) and WNVpro (27%) than for NS3pro (53%).

Knowledge of the three-dimensional structure of the target protein is important for any attempt at rational drug design. In the case of DENpro, however, it is very uncertain whether low molecular weight inhibitors can at all drive the protease toward the closed state. This is an important question, as some of the current drug design efforts are based on models of DENpro that use the closed conformation of WNVpro as a template,[18−22] while others use an open conformation,[23−26] structures that have been retracted since,[27,28] or no model at all.[5,29−32]

Despite intense efforts,[6,33] crystal structures of DENpro with a bound inhibitor have remained elusive. In any case, the ease with which crystal contacts alter the conformation of NS2B-C underlines the importance of structure analysis in solution. Therefore, we set out to determine whether, in solution, DENpro can assume a closed state that is similar to the one observed for WNVpro and whether this conformation can be induced by low-molecular weight inhibitors. Here and in the following, "DENpro" refers to the construct of serotype 2 used in the present work (Figure 1C).

Unfortunately, DENpro produces NMR spectra of poor quality with substantial peak overlap and many signals missing due to excessive line broadening. Therefore, we addressed these questions using novel approaches in which the protein was tagged with paramagnetic lanthanides for the observation of long-range structure restraints. The results show unambiguously that an ensemble of open conformations exist in the absence of inhibitors, while positively charged low molecular weight inhibitors (Figure 2) can readily induce a closed conformation related to that reported for WNVpro.

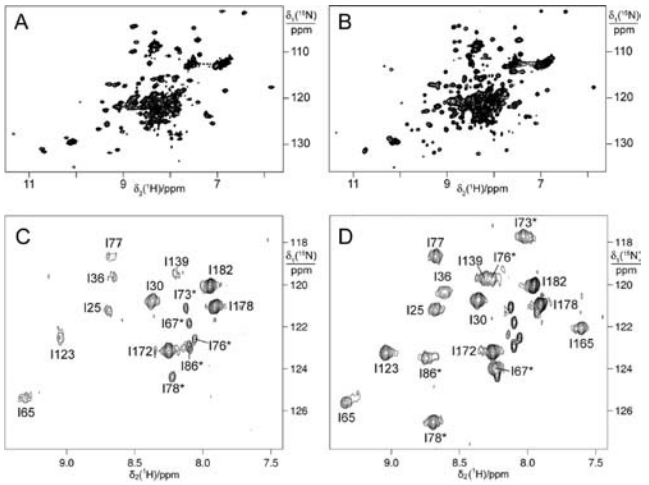

Figure 3. ^{15}N-HSQC spectra of DENpro at pH 6.9 and 25 °C. (A) 1 mM solution of uniformly ^{15}N-labeled DENpro without inhibitor. (B) Same as (A) but with a 5-fold excess of inhibitor **1**. (C) 50 μM solution of selectively ^{15}N-isoleucine labeled DENpro without inhibitor. The spectral region shown corresponds to the region of intense signal overlap in (A). Cross-peaks are labeled with their resonance assignments. Asterisks mark residue numbers of NS2B. (D) Same as (C) but in the presence of a 10-fold excess of inhibitor **1**. Some of the narrow cross-peaks from NS2B identified in (C) are still present in (D), suggesting that not all protein could be saturated with inhibitor due to degradation.

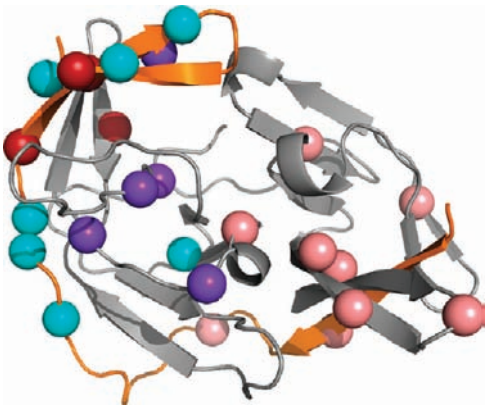

Figure 4. Conformational exchange in the microsecond to millisecond time range affects NMR resonances mostly in the C-terminal β-barrel associated with NS2B-C rather than in the N-terminal β-barrel. The figure shows the model of the closed conformation of DENpro oriented such that the N- and C-terminal β-barrels are in the right and left halves, respectively. NS2B is shown in orange and NS3pro in gray. Balls identify residues for which assignments were attempted in the absence of inhibitor. They are color coded as in Figure S11 (Supporting Information) to reflect changes in the intensity and chemical shift of the ^{15}N-HSQC cross-peaks after addition of **1**. Red: significant change in peak height; blue: significant change in chemical shift; purple: cross-peak observable only in the presence of **1**; pink: no significant spectral change.

RESULTS

Resonance Assignments. In the absence of an inhibitor, the NMR spectrum of DENpro is unsuitable for resonance assignments by conventional techniques as many of the signals are much broader than expected for the molecular weight of the protein or even missing, indicating conformational exchange on the micro- to millisecond time scale (Figure 3A and C). Besides excessively broad lines (e.g., of residues 25, 36, 65, 77, and 139 in Figure 3C), some of the signals are very narrow (e.g., residues 67*, 73*, 76*, 78*, and 86* in Figure 3C). In the presence of inhibitor, the cross-peak intensities were much more uniform (Figure 3B and D). We thus set out to assign the backbone resonances for the complex with inhibitor **1** (Figure 2). Even with inhibitor and using ^{2}H/^{15}N/^{13}C-labeled samples, however, the assignments by conventional 3D NMR experiments were hampered by limited sensitivity and severe signal overlap in the spectral region centered around [δ_1(^{15}N) = 122 ppm/δ_2(^{1}H) = 8.2 ppm] (Figure 3B). In this situation, significant assistance came from two sets of combinatorially isotope-labeled samples prepared by cell-free protein synthesis.[8] The first set comprised five samples with different combinations of ^{15}N-labeled amino acids to identify the residue type of each ^{15}N-HSQC cross-peak.[37−39] The second set of five samples used different combinations of ^{15}N/^{13}C-labeled amino acids, while all other amino acids were ^{15}N-labeled. Using 2D HN(CO) spectra, this set identified the type of the preceding residue for each ^{15}N-HSQC cross-peak.

In addition, ^{15}N-HSQC peaks were assigned by site-directed mutagenesis using selectively ^{15}N-labeled samples to minimize the spectral overlap.[8] Thus, all ^{15}N-HSQC cross-peaks of isoleucine residues were assigned by preparing 16 samples, where each isoleucine residue was mutated to valine one at a time. The decrease in intensity of individual cross-peaks identified their assignment (Figure S1, Supporting Information). The cross-peaks of the serine residues at positions 68*, 70*, 71*, 79*, 83*, and 85* were assigned similarly by mutation to alanine (Figure S2, Supporting Information), and the ^{15}N-HSQC cross-peaks of Arg55* and Arg60* were assigned by mutation to lysine (Figure S3, Supporting Information). The cross-peak of Thr77* was identified by a 2D HN(CO) spectrum of a sample labeled with ^{15}N-threonine and ^{15}N/^{13}C-isoleucine. Finally, resolved ^{15}N-HSQC cross-peaks were assigned by PCSs induced by two different metal ions in two different tags at three different sites (discussed further below). The combined effort led to the assignment of the ^{15}N-HSQC cross-peaks of 50% of the protein with bound **1** (summarized in Figure 1C).

Conformational Exchange. The selectively ^{15}N-labeled samples of the single-residue mutants provided a limited number of resonance assignments also in the absence of inhibitor. Most of the narrow resonances at chemical shifts characteristic of random coil peptides were from residues of the C-terminal segment of NS2B, NS2B-C (for example, the cross-peaks of Ile67*, Ile76*, Ile78*, and Ile86* in Figure 3C). The narrow line widths of these signals indicate high mobility of the NS2B peptide segment between Ile67* and Ile86*, in agreement with the crystal structure of DENpro where NS2B-C is dissociated from NS3pro.[6] In the presence of **1**, however, this segment was immobilized, as the line widths of the cross-peaks of NS2B-C became comparable to those of the cross-peaks of NS3pro (Figure 3D). In addition, the chemical shift dispersion of the NS2B-C cross-peaks increased, and weak cross-peaks of NS3pro residues became more intense. The uniform cross-peak intensities suggest that the inhibitor triggers the association of NS2B-C with NS3pro into a structure where conformational exchange manifested by unusually narrow or broad lines is suppressed and NS2B-C and NS3pro tumble in solution as a single structural entity. Inhibitor **2** elicited very similar spectral changes in the ^{15}N-HSQC spectrum, suggesting that **2** promotes a similar conformational change as **1** (Figure S10, Supporting Information).

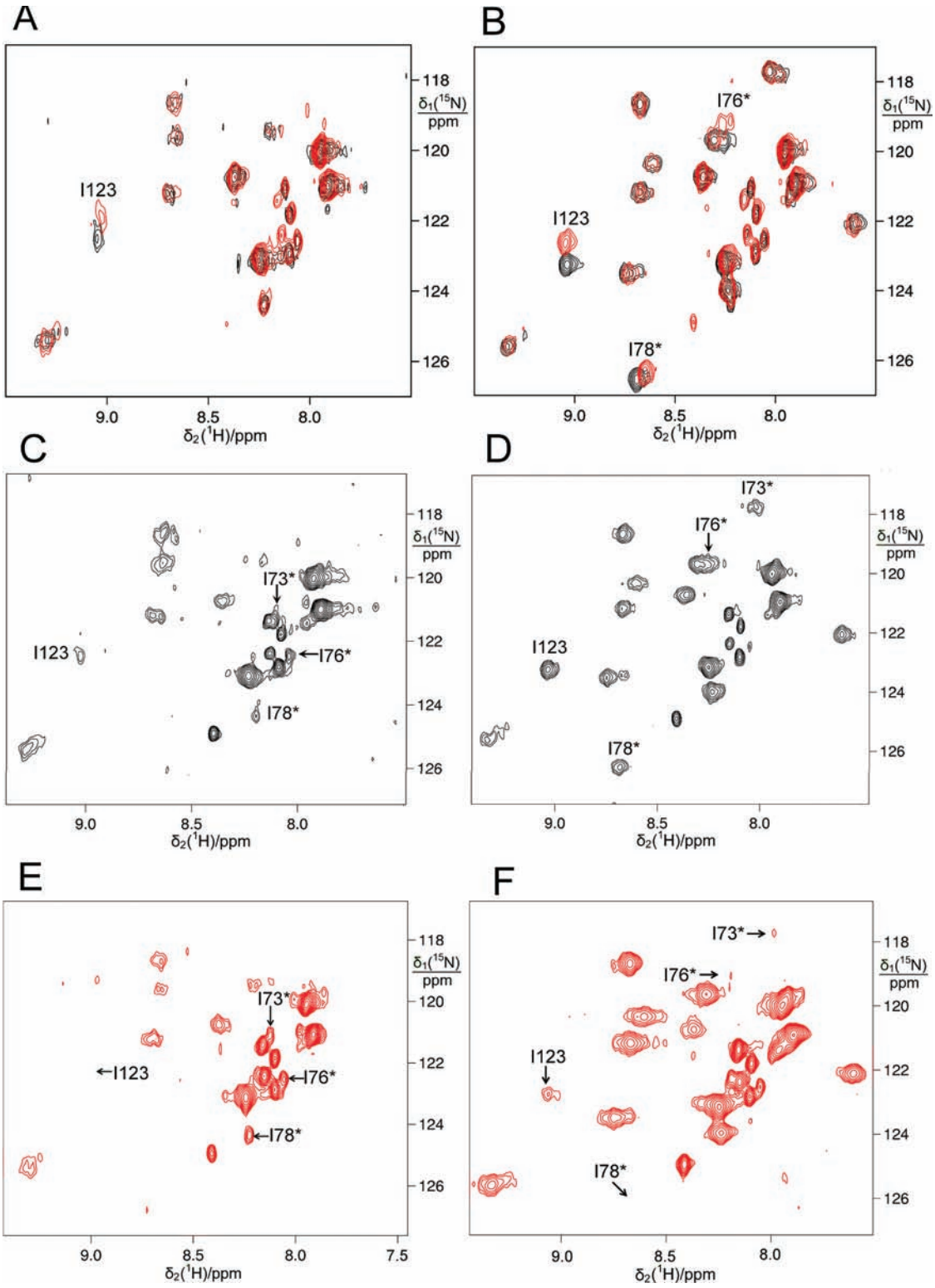

Figure 5. Paramagnetic relaxation enhancements from a site-specifically bound $[Gd(DPA)_3]^{3-}$ complex affect NS2B-C residues differently in the closed and open states. The figure shows ^{15}N-HSQC spectra of ^{15}N-isoleucine labeled wild-type and mutant (Lys117Arg/Thr122Arg) DENpro. Left-hand and right-hand panels show spectra in the absence and presence of inhibitor **1**, respectively. (A and B) Superimposition of spectra of wild-type DENpro (black) and of the mutant Lys117Arg/Thr122Arg (red). Protein concentrations were 50 and 60 μM, respectively. Only a few cross-peaks (identified by assignments) are significantly affected by the mutation. (C and D) ^{15}N-HSQC spectra of 60 μM solutions of ^{15}N-isoleucine labeled wild-type DENpro in the presence of 0.3 mM $[Gd(DPA)_3]^{3-}$. These control experiments show that, in the wild-type protein, $[Gd(DPA)_3]^{3-}$ does not bind near any of the isoleucine residues. (E and F) Same as C and D, except for DENpro(Lys117Arg/Thr122Arg). Labels identify cross-peaks that show large PREs in the presence of inhibitor (compare B and F).

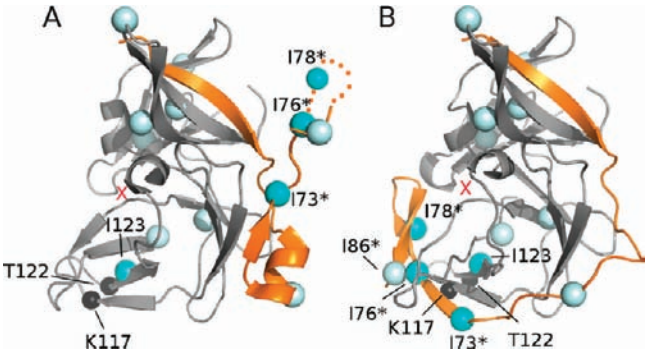

Figure 6. Isoleucine residues of NS2B in DENpro are predicted to experience PREs due to $[Gd(DPA)_3]^{3-}$ binding at the site of the double mutation Lys117Arg/Thr122Arg in the closed state but not in the open state. The nitrogen atoms of the mutation site (residues 117 and 122) are drawn as black spheres. The nitrogen atoms of the four isoleucine residues which experience PREs due to $[Gd(DPA)_3]^{3-}$ in the mutant are drawn as blue balls, while isoleucines without significant PREs are identified by light blue balls. NS2B and NS3pro are displayed as orange and gray ribbons, respectively. (A) Crystal structure of the inhibitor-free DENV protease (PDB accession code 2FOM). As electron density was missing for parts of NS2B including Ile78*, the sphere representing Ile78* has been drawn at a position nearby. (B) Structure of inhibitor-bound DENpro modeled on the closed conformation of inhibitor-bound WNVpro. This structure explains the PREs observed for the NS2B residues Ile78*, Ile76*, and Ile73*. The amide of Ile86* did not show a measurable PRE. It is located at least 2 Å further away from the metal binding site than any of the isoleucine residues showing PREs. The location of the active site is marked with a red cross.

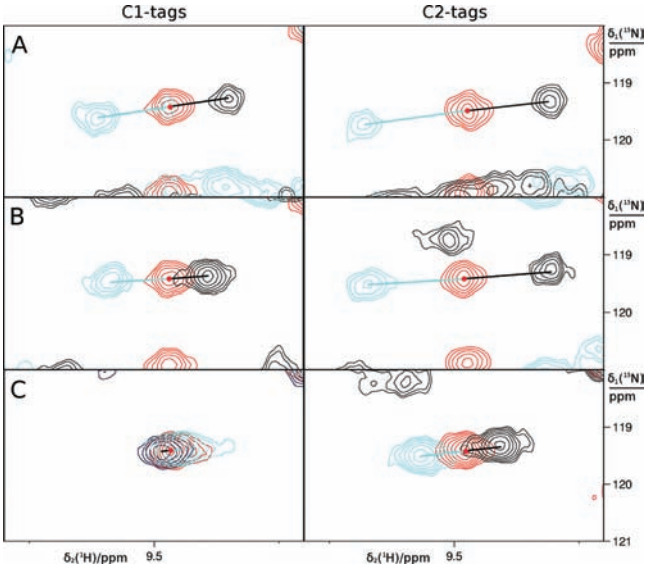

Figure 7. Pseudocontact shifts observed for the ^{15}N-HSQC cross-peak of Phe116 in 12 different samples. Panels A–C correspond to the cysteine mutants A–C. The left-hand and right-hand panels show the spectra of mutants ligated with the C1- and C2-tag, respectively. The diamagnetic cross-peaks (tags loaded with Y^{3+}) are shown in red and marked with a red dot. The spectra measured with Tm^{3+} and Tb^{3+} tags are shown in black and cyan, respectively. The cross-peaks are linked by lines indicating the pseudocontact shifts. The spectra were recorded of 0.1–0.2 mM solutions of uniformly ^{15}N-labeled DENpro in NMR buffer (pH 6.5) at 25 °C, using an 800 MHz NMR spectrometer.

Interestingly, residues for which the ^{15}N-HSQC cross-peaks changed significantly in chemical shift or line width upon addition of **1** are almost all located either in NS2B-C or in the C-terminal β-barrel of the protease, for which dissociation of NS2B-C from NS3pro causes a greater change in chemical environment than for the N-terminal β-barrel (Figures 4 and S11, Supporting Information). The conformational equilibrium leading to the broadening and disappearance of NMR signals is thus most likely coupled to the association–dissociation equilibrium between NS2B-C and NS3pro.

Structural Analysis of the Closed Conformation by PREs. To test the hypothesis that an inhibitor at the substrate binding site causes NS2B-C to wrap around NS3pro and approach the active site, we first produced a binding site for a paramagnetic lanthanide ion (Ln^{3+}) complex with dipicolinic acid (DPA), $[Ln(DPA)_3]^{3-}$,[40] by preparing the double mutant Lys117Arg/Thr122Arg. These residues were chosen because they fulfill the criteria for creating binding sites for $[Ln(DPA)_3]^{3-}$ complexes: their side chains are near each other in the crystal structures of DENpro of serotypes 1 and 2,[6,7] they project into solution in the same direction, and there is no negatively charged side chain nearby that could form a salt-bridge with the engineered arginine residues.[40–42]

Binding of the strongly paramagnetic $[Gd(DPA)_3]^{3-}$ complex to the engineered mutation site presents a source of paramagnetic relaxation enhancements (PRE) for the nuclear spins nearby.[41,42] PREs are manifested in the NMR spectrum by line broadening and decrease very steeply with increasing distance of the nuclear spins from the unpaired electrons of the Gd^{3+} ion. The $[Gd(DPA)_3]^{3-}$ binding site was designed at a location where PREs would be expected to be observable for NS2B-C in the closed but not in the open state. This prediction was borne out by experiment.

Control experiments showed that the double mutation Lys117Arg/Thr122Arg changed the NMR spectrum only a little relative to that of the wild-type, indicating that the mutations did not affect the fold of the protein (Figure 5A and B). Addition of a 5-fold excess of $[Gd(DPA)_3]^{3-}$ to the wild-type protein did not lead to significant attenuation of any of the cross-peaks in the absence or presence of inhibitor, confirming the absence of a natural binding site for $[Ln(DPA)_3]^{3-}$ complexes near any of the isoleucine residues probed by the experiments (Figure 5C and D). In contrast, the double mutant Lys117Arg/Thr122Arg led to significant cross-peak attenuation in the presence of $[Gd(DPA)_3]^{3-}$. In the absence of **1**, the cross-peak of Ile123 disappeared due to PRE from $[Gd(DPA)_3]^{3-}$ (Figure 5E). In the presence of **1**, the PREs also significantly attenuated the cross-peaks of the NS2B-C residues Ile73*, Ile76*, and Ile78*, showing that the inhibitor brought these residues into proximity of the $[Gd(DPA)_3]^{3-}$ binding site (Figure 5E).

These results are readily understood if DENpro assumes open and closed conformations similar to the crystal structures of WNVpro (Figure 1). Open conformations such as that observed in the crystal structure of DENpro in the absence of inhibitor[6] position NS2B-C far from the engineered $[Ln(DPA)_3]^{3-}$ binding site, which is near Ile123 (Figure 6A). In contrast, the closed conformation of Figure 1B positions Ile73*, Ile76*, and Ile78* near the designed binding site of the $[Gd(DPA)_3]^{3-}$ complex (Figure 6B), in agreement with our experimental results.

Analysis of the Closed State by PCSs. To analyze the closed conformation induced by the presence of **1** in more detail, we produced single-cysteine mutants in the more stable N-terminal

Table 1. Effective $\Delta\chi$ Tensor Parameters of the 12 Different Lanthanide Tags[a]

	mutant A				mutant B				mutant C			
	C1		C2		C1		C2		C1		C2	
	Tm^{3+}	Tb^{3+}	Tm^{3+}	Tb^{3+}	Tm^{3+}	Tb^{3+}	Tm^{3+}	Tb^{3+}	Tm^{3+}	Tb^{3+}	Tm^{3+}	Tb^{3+}
$\Delta\chi_{ax}/10^{-32}$ m^3	10.6	−10.3	−17.1	−22.6	7.6	−10.8	11.8	−13.8	−12.8	16.3	11.5	−20.3
$\Delta\chi_{rh}/10^{-32}$ m^3	2.3	−4.4	−10.6	−12.6	1.1	−2.7	2.9	−3.6	−3.6	7.4	3.0	−5.9

[a] The $\Delta\chi$ tensors were determined by fits to the NS3pro part (including residues 55*−57* of NS2B) of the model structure of the closed state (Figure 1B).

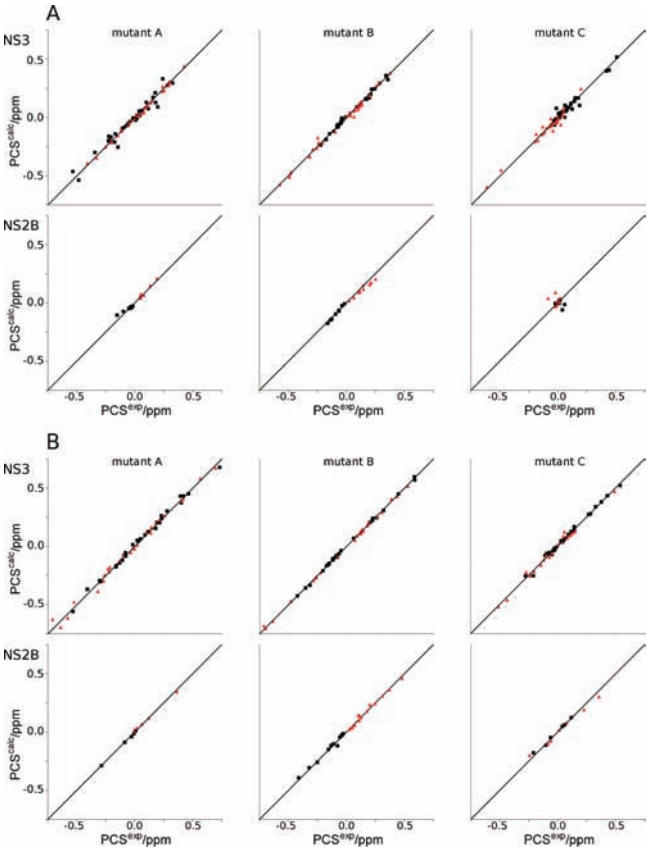

Figure 8. Calculated versus experimental pseudocontact shifts, using the model of the closed conformation (Figure 1B) for fitting $\Delta\chi$ tensors to NS3pro. PCSs of Tb^{3+} and Tm^{3+} are indicated in red and black, respectively. Straight lines mark unity slopes. Separate correlations are shown for mutants A−C (as indicated above the plots). The PCSs of NS2B-C (shown in the panels underneath the NS3pro correlations) were not used in the fits of the $\Delta\chi$ tensors. (A) Correlations of PCSs obtained with the C1-tag. (B) Correlations of PCSs obtained with the C2-tag.

β-barrel of DENpro and attached lanthanide tags. Three different mutants were produced, Ala57*Cys, Ser34Cys, and Ser68Cys (positions labeled A, B, and C in Figure 1). Each mutant was expressed as a uniformly ^{15}N-labeled sample and ligated with the C1-tag[36] loaded with Tm^{3+}, Tb^{3+}, or Y^{3+}, where the samples with Y^{3+} served as the diamagnetic reference. Compound **1** was added to induce the closed conformation. Additional samples of each uniformly ^{15}N-labeled protein mutant were prepared using the C2-tag loaded with the same metal ions. Using two different tags with two different paramagnetic metal ions for each of the three cysteine mutants led to 12 different paramagnetic samples. In addition, selectively ^{15}N-isoleucine labeled samples of all three cysteine mutants were prepared and tagged with C1−Tb^{3+} and C1−Y^{3+} to obtain data for some of the cross-peaks that were strongly overlapped in the ^{15}N-HSQC spectra of the uniformly ^{15}N-labeled samples.

Table 2. Quality Factors of the Tensor Fits to the Model of the Closed State and to the Open Conformation[a]

	mutant A		mutant B		mutant C	
	C1	C2	C1	C2	C1	C2
NS3pro	0.031	0.007	0.007	0.001	0.040	0.007
	(0.12)	(0.057)	(0.058)	(0.038)	(0.060)	(0.025)
NS2B-C	0.039	0.005	0.026	0.007	2.9	0.39
	(1900)	(4900)	(1.3)	(1.0)	(3.1)	(2.7)
all	0.031	0.007	0.009	0.002	0.060	0.010
	(84)	(200)	(0.13)	(0.12)	(0.066)	(0.17)

[a] Calculated as the root-mean-square deviation between experimental and back-calculated PCSs divided by the root-mean-square of the experimental PCSs. The PCSs from Tm^{3+} and Tb^{3+} tags were combined. The values in the top lines are for the fits to NS3pro in our model of the closed conformation (including residues 55*−57* of NS2B), and the values underneath (in brackets) are for the structure 2FOM.

The Tm^{3+} and Tb^{3+} tags served to induce pseudocontact shifts in the protein. For backbone amides sufficiently close to all three tagging sites, up to 12 different PCSs were observed (Figure 7). In total, 479 PCSs were measured (Tables S1−S3, Supporting Information). The PCSs induced by each tag were interpreted by $\Delta\chi$ tensors fitted to the coordinates of NS3pro and the N-terminal part of NS2B that is structurally conserved in the crystal structures (Table 1).[6,7] The $\Delta\chi$ tensors were subsequently used to predict the PCSs of NS2B-C and check the agreement with the experimental PCSs observed for NS2B-C.

Using our model of the closed state (Figure 1B) produced excellent $\Delta\chi$ tensor fits (Figure 8, Table 2). Although the magnitude of the $\Delta\chi$ tensor associated with a given lanthanide is a priori independent of the chirality of the tag, different effective $\Delta\chi$ tensors were observed for the C1- and C2-tags (Table 1 and Figure 9). These differences are expected to arise from different ranges of conformational freedom of the tether between tag and protein in the diastereomeric protein-tag adduct, leading to different degrees of PCS averaging in the protein and, hence, different effective $\Delta\chi$ tensors if the tensors are determined from the PCSs of the protein.[36] The quality of the fits to NS3pro (Table 2) indicated that the effective $\Delta\chi$ tensors could be used to assess the conformation of NS2B-C. Predicting the PCSs of

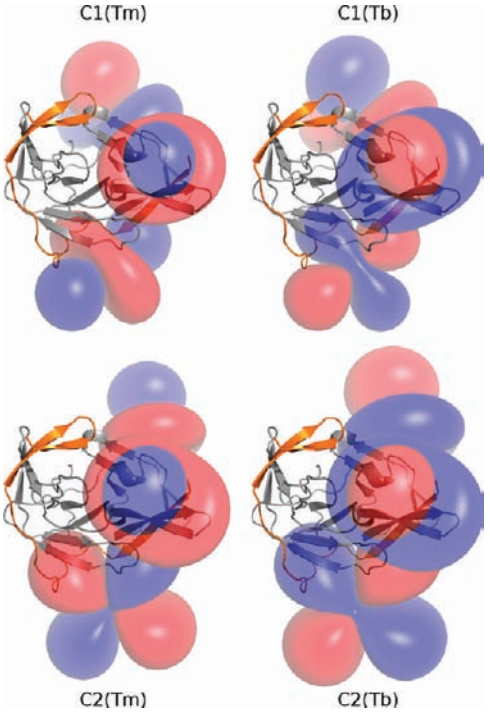

Figure 9. Effective $\Delta\chi$ tensors derived from PCSs observed in NS3pro differ from each other. For visualization, the 12 $\Delta\chi$ tensors produced by the different mutants, tags, and lanthanide ions are represented by isosurfaces of constant PCS plotted on a ribbon drawing of the DENpro model of the closed state. The blue and red lobes correspond to PCS isosurfaces contoured at +1 ppm and −1 ppm, respectively. Isosurfaces resulting from the same lanthanide tag at the mutant sites A−C are plotted on the same structure, although they were determined with different protein samples. The mutation site of A is located at the bottom of the structure, B in the middle, and C at the top. Top and bottom panels: isosurfaces produced by C1- and C2-tags, respectively. Left and right panels: isosurfaces produced by Tm^{3+} and Tb^{3+}, respectively. Tm^{3+} and Tb^{3+} produce related $\Delta\chi$ tensors of opposite sign, whereas C1- and C2-tags produce more different $\Delta\chi$ tensors.

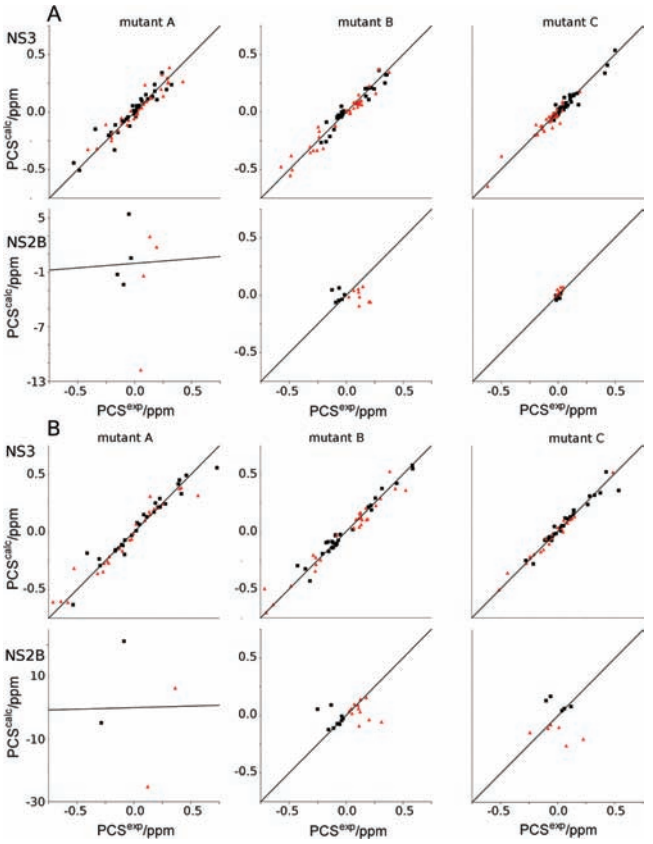

Figure 10. Same as Figure 8, except using the open conformation of DENpro (PDB code 2FOM) for fitting the $\Delta\chi$ tensors to NS3pro and back-calculating the PCSs.

NS2B-C led to very good agreement with the experimental data (Figure 8), whereas the open conformation (Figure 1A) explained the experimental PCSs of NS3pro less well and the PCSs of NS2B-C not at all (Figure 10, Table 2).

The PCSs not only pinned down the conformation of NS2B-C in the closed state but also resolved the more subtle conformational differences between NS3pro in the open and closed states, as reflected by the crystal structure 2FOM[6] and the model of Figure 1B, respectively. The C^{α} rmsd between NS3pro in our model and in the 2FOM structure is less than 2.2 Å for 150 superimposed residues. Despite the close structural similarity for this part of DENpro, the $\Delta\chi$ tensor fits to NS3pro were significantly better for our model (Figures 8) than for the crystal structure 2FOM (Figure 10, Table 2), showing that NS3pro conformation of the model is a more faithful representation of the closed state.

Resonance Assignments Using PCSs. The excellent match between predicted and experimental PCSs (Figure 8) and the availability of many PCSs for resolved ^{15}N-HSQC cross-peaks allowed the assignment of an additional 12 ^{15}N-HSQC cross-peaks which were well-resolved in the spectrum but could not be assigned earlier because of limited sensitivity or because the signals from the sequentially neighboring residues could not be assigned (Figure 11). As far as the additional assignments belonged to NS3pro and the N-terminal part of NS2B, the PCSs of these additionally assigned cross-peaks were included in a revised PCS data set. This final data set was used to fit the $\Delta\chi$ tensors as reported in Table 1 and Figures 8−10.

Inhibitor Binding. The inhibitor **1** is a well-known inhibitor for arginine-specific serine proteases with which it reacts to form a covalent ester bond.[43,44] We ascertained reaction of **1** with the active-site residue Ser135 of DENpro by the following observations: (i) addition of inhibitor **1** to the protease released the yellow *p*-nitrophenolate anion, the identity of which was confirmed by 1D NMR spectroscopy; (ii) titration of the protein with *p*-guanidino-benzoate did not lead to changes in the ^{15}N-HSQC spectrum, indicating no binding; (iii) mass spectrometry showed that only the *p*-guanidino-benzoic acid moiety remained bound to the protein (Figure S6, Supporting Information); and (iv) preparation of the enzymatically inactive mutant Ser135Ala confirmed that **1** produced no significant spectral changes in the ^{15}N-HSQC spectra of uniformly ^{15}N-labeled protein, indicating the absence of binding (Figure S5, Supporting Information). In addition, the hydrolysis of **1** was much slower in the presence of the active site mutant, akin to the rate of hydrolysis in water without enzyme catalysis.

The ester bond between Ser135 and *p*-guanidino-benzoate pins the inhibitor to the active site. According to our model (Figure 1B), the *p*-guanidino-benzoic acid moiety bound to Ser135 is too small to form any significant direct contacts with

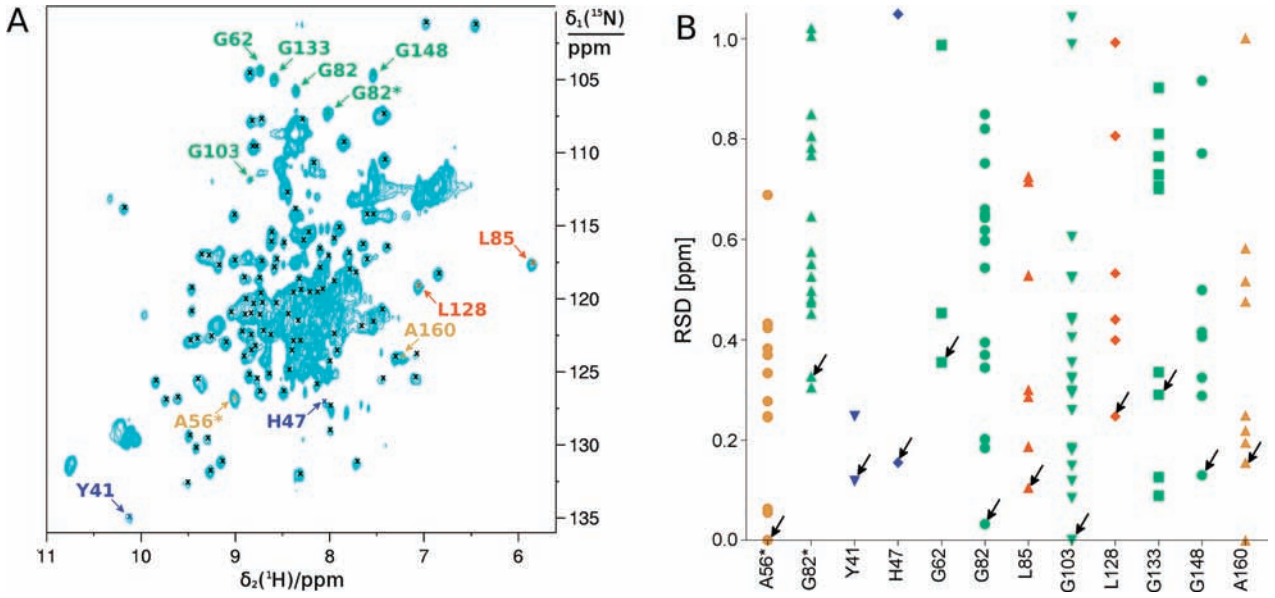

Figure 11. Resonance assignments by multiple PCSs from multiple tags. (A) ^{15}N-HSQC spectrum of uniformly ^{15}N-labeled DENpro in the presence of a 5-fold excess of **1**. The black points mark the cross-peaks assigned by 3D NMR spectra of a ^{2}H/^{15}N/^{13}C-labeled sample. The color-labeled peaks were assigned by a best fit of calculated and experimental PCSs, aided by the fact that the amino acid types of the corresponding residues as well as of the sequentially preceding residues were known from combinatorial ^{15}N-labeling.[37−39] Different colors mark different residue types. (B) Root square deviation (RSD) of the calculated and experimental PCSs of the cross-peaks assigned by PCSs. The plot shows all RSD values calculated for the different residues of a certain type present in the model structure of Figure 1B. The arrows identify the RSD value of the final assignment made after inspection of the 3D NMR data for plausible connectivities.

NS2B-C. It is thus all the more remarkable that inhibitor **1** can induce the closed state in DENpro.

***β*-Hairpin Conformation of NS2B-C.** While PCSs provide powerful long-range structure restraints, nuclear Overhauser effects (NOE) offer valuable short-range restraints. Analysis of the 3D NOESY−^{15}N-HSQC spectrum, however, was hampered by limited signal-to-noise ratio and difficulties in assigning any resonances beyond the backbone amides. A single H^N−H^N NOE between the β-strands of NS2B-C could be identified (Thr77* to Ser85*). Inspection of our model shows that this is also the only interstrand H^N−H^N NOE expected in the β-hairpin of NS2B-C. In addition, we analyzed the cross-peaks at the chemical shift of the water resonance. Under the conditions used (pH 6.9, 25 °C), most of these would arise from ^{1}H exchange between water and amide protons. Amide protons involved in the interstrand H-bonds predicted by the model of the closed state (Figure 1B) indeed showed smaller cross-peak intensities with the water than non-hydrogen-bonded amides (Figure S8, Supporting Information). The only exceptions were Ile76* and Ile78*, which showed small exchange cross-peaks although the model predicts no H-bonds for them. This observation was expected, as the side chain of isoleucine residues is known to slow down amide proton exchange rates more than any other amino acid side chain.[45]

■ DISCUSSION

The existence of a closed state in dengue NS2B-NS3pro has been enigmatic ever since very different crystal structures were reported for the corresponding NS2B-NS3pro construct of the West Nile virus protease. While the enzymatic activities of the proteases depend critically on NS2B, solution studies indicated that the C-terminal segment of NS2B, NS2B-C, is mostly dissociated from NS3pro in the dengue virus protease but not in the WNV enzyme.[8,16] The present data show that, in solution, a low molecular weight inhibitor can tie NS2B-C to NS3pro near the substrate binding site as anticipated for the fully active form of the enzyme. Furthermore, all our data indicate that NS2B-C forms a β-hairpin conformation very similar to that observed in the crystal structures of WNV NS2B-NS3pro with bound inhibitors. Finally, our data demonstrate that, even though the fold of NS3pro is conserved between the open and closed conformation of the enzyme, there are nonetheless subtle conformational differences, as shown by an improved fit of the PCSs to the model of the closed conformation as opposed to the crystal structure of an open conformation. It has previously been observed that NS3pro exhibits NS2B-independent activity with small chemical substrates such as *N*-α-benzoyl-L-arginine-*p*-nitroanilide, whereas the activity toward peptide substrates is stimulated significantly in the presence of NS2B.[4,46] While binding of peptide substrates to the substrate binding site may be stabilized by contacts with NS2B, peptide binding may also be promoted by the particular conformation of NS3pro induced by the binding of NS2B-C to NS3pro.

Driving Force for Conformational Change. It is remarkable that the inhibitor **1** is able to elicit the conformational change of DENpro to the closed conformation, despite the fact that, following ester bond formation with Ser135, the remaining *p*-guanidino-benzoate moiety is too small to form direct contacts with NS2B-C. We attribute this effect to electrostatic attraction between the positive charge of the inhibitor and the tip of the NS2B-C β-hairpin (which carries two or even three negatively charged, sequentially neighboring residues in all four dengue serotypes[10]) toward the substrate binding site of the protease. It is therefore not unexpected that inhibitor **2**, by virtue of its positively charged imidazoline groups, equally appears to induce

the closed state. This notion is also consistent with the fact that DENpro specifically cleaves peptides with a positively charged residue in the P1 site[47] and that the activity of the protease decreases with increasing salt concentration.[4,5,48] The important conclusion is that the closed conformation should be used for modeling complexes with positively charged inhibitors, whereas uncharged or negatively charged inhibitors may be more likely to target an open conformation.

Paramagnetic Labeling for Structure Analysis. The potential of paramagnetic lanthanides in structural biology has been recognized long ago,[49−51] but to realize this potential in full requires multiple lanthanide binding sites.[52] This prediction is borne out in the present work, where PCSs generated by different paramagnetic lanthanide tags at different sites proved extraordinarily powerful for analyzing the fold of DENpro. As conformational exchange broadened the NMR signals of DENpro, with even the ^{15}N-HSQC spectrum being of poor quality, we relied almost exclusively on PCSs to obtain structural information from resolved ^{15}N-HSQC cross-peaks in the absence of complete resonance assignments. Owing to their long-range nature, lanthanide-induced PCSs are ideally suited for this purpose. The $\Delta\chi$ tensor of each tag is centered on the lanthanide ion and effectively presents a coordinate frame anchored to the protein. As a $\Delta\chi$ tensor is defined by only eight parameters (its axial and rhombic components, the x, y, z coordinates of the metal ion, and three Euler angles to relate the orientation of the tensor to the protein coordinates), it can be determined from a minimum of eight PCSs measured for nuclear spins located at known positions in the 3D structure of the protein. Therefore, our strategy does not require complete resonance assignments of the protein NMR spectrum. Once the $\Delta\chi$ tensors have been established, the PCSs measured for a nuclear spin present strong restraints for its location relative to the coordinate systems of the $\Delta\chi$ tensors and, therefore, to the 3D structure of the protein.

Figure 9 shows that all 12 $\Delta\chi$ tensors obtained for the different mutants, tags, and metal ions were different from each other, but very different tensor orientations that would produce the most conclusive structural information were obtained mainly by using different tagging sites. In practice, the choice of positioning the lanthanide tags was limited only by the solvent accessibility of the cysteine mutants and their location in the more rigid N-terminal β-barrel of NS3pro to avoid the possibility of structural distortions in the more flexible C-terminal β-barrel. This flexibility in the choice of tagging site makes our strategy widely applicable to proteins devoid of structurally or functionally essential cysteine residues.

This is the first time that so many paramagnetic lanthanide tags have been used to analyze a protein. As $\Delta\chi$ tensors of lanthanides at different sites cannot be linearly proportional to each other (as the case may be for different lanthanides at the same site, Figure 9), multiple lanthanide sites offer greatly enhanced information content. In the present study, the resulting PCS data sets allowed not only a robust assessment of the 3D fold of the protein but also assignments of ^{15}N-HSQC cross-peaks by comparison of experimental PCSs with predictions based on the structure of the protein. Previous PCS-based assignment strategies were limited to PCSs generated by a single lanthanide binding site and therefore depended on additional NMR data beyond PCS and residue-type information.[53,54] It is clear that multiple lanthanide tagging sites will equally enhance the accuracy of 3D structure determinations of protein−protein complexes that are based on lanthanide-induced PCSs.[55,56]

Paramagnetic relaxation enhancements are exquisitely sensitive for the detection of rare conformations.[57] This project employed an alternative gadolinium-labeling scheme that does not depend on single cysteine residues, generating instead a binding site for the $[Gd(DPA)_3]^{3-}$ complex by introducing two positively charged amino acid residues in close spatial proximity. The paramagnetic relaxation enhancements measured with this probe did not only agree with the closed state of the protease in the presence of **1**, but also showed that in solution, the C-terminal β-hairpin of NS2B does not populate the open state conformation displayed by the crystal structure 2FOM[6] to any significant extent. Even less than 5% population of this particular open conformation would have resulted in significant paramagnetic relaxation enhancements, which we did not observe. The NMR data show that, without inhibitor, NS2B-C is highly mobile in solution, while the particular conformation observed in the crystal structure is visited rarely.

CONCLUDING REMARKS

A more quantitative assessment of the accuracy of our model of the closed state will be possible once a crystal structure of DENpro with a bound inhibitor becomes available. Interestingly, we found that DENpro, but not the active-site mutant DENpro Ser135Ala, is prone to cleavage after Trp5 of NS3pro (Figure S7, Supporting Information). While this activity may not be of physiological significance, the resulting sample heterogeneity could interfere with crystallization of DENpro.

The methods applied in this project make two important advances for NMR studies of the large class of proteins that are poorly soluble, suffer from dynamic NMR line broadening, or show only a limited number of resolved cross-peaks in the ^{15}N-HSQC spectrum for other reasons. First, we were able to derive all the critical structural information from changes in backbone amide chemical shifts (PCSs) in straightforward ^{15}N-HSQC spectra rather than from NOEs, which would have required laborious analysis of spectra that are far less sensitive, take much longer to record, and, for the most part, are impossible to interpret in the absence of comprehensive resonance assignments. Second, we were able to use the PCSs to assign well-resolved ^{15}N-HSQC cross-peaks with the help of a structural model of the protein, even though many of the ^{15}N-HSQC cross-peaks remained unassigned due to spectral overlap. The ability to assign well-resolved cross-peaks in the ^{15}N-HSQC spectrum is of obvious interest in drug discovery projects, where the approximate binding sites of small compounds can be gleaned simply from chemical shift changes of amide protons in close spatial proximity. With the advent of improved lanthanide tags (for a review, see ref 58), we expect that PCSs will become a routine tool for resonance assignments and structure analysis of proteins that were hitherto considered to give too poor NMR spectra.

Finally, the $\Delta\chi$ tensors determined in the present work open an avenue to determine the conformations of low-molecular weight compounds binding to DENpro by measuring their PCSs in straightforward 1D NMR spectra.[59] We are currently testing different ligands using this approach.

ASSOCIATED CONTENT

Supporting Information. Complete reference 18, experimental protocols, ^{15}N-HSQC spectra of each of the 16 Ile to Val and 7 Ser to Ala mutants of DENpro without and with

inhibitor **1**, ^{15}N-HSQC spectra of two Arg to Lys mutants of DENpro without and with inhibitor **1**, comparison between ^{15}N-HSQC spectra of the mutants A−C with diamagnetic tags and the ^{15}N-HSQC spectrum of the wild-type protein, PCSs of backbone amide protons of ^{15}N-labeled DENpro, ^{15}N-HSQC spectrum of the DENpro mutant Ser135Ala in the presence of inhibitor **1**, mass spectra of DENpro with and without inhibitor **1** and of DENpro (mutant Lys15Ala), amide proton exchange data of NS2B, display of the gradients of steepest descent of local quality factors of the PCSs in NS2B, ^{15}N-HSQC spectrum of DENpro with inhibitor **2**, backbone amide ^{1}H and ^{15}N chemical shifts of DENpro, and comparison of peak intensities and chemical shifts between the open and closed state. This material is available free of charge via the Internet at http://pubs.acs.org.

AUTHOR INFORMATION

Corresponding Author

gottfried.otting@anu.edu.au

Present Addresses

[§]MRC Laboratory of Molecular Biology, Hills Road, Cambridge, CB2, 0QH, U.K.

ACKNOWLEDGMENT

We thank Dr. Siew-Pheng Lim at the Novartis Institute for Tropical Diseases (NITD) for the initial construct of the dengue virus protease, the inhibitor **2**, and for careful reading of the manuscript and Drs. Ruhu Qi and Xun-Cheng Su for help with primer design, sample preparation, and NMR spectroscopy. Financial support by NITD and the Australian Research Council, including a Future Fellowship to T.H., is gratefully acknowledged.

REFERENCES

(1) Kuno, G. *Rev. Med. Virol.* **2007**, *17*, 327–341.

(2) Guzman, M. G.; Halstead, S. B.; Artsob, H.; Buchy, P.; Farrar, J.; Gubler, D. J.; Hunsperger, E.; Kroeger, A.; Margolis, H. S.; Martínez, E.; Nathan, M. B.; Pelegrino, J. L.; Simmons, C.; Yoksan, S.; Peeling, R. W. *Nat. Rev. Microbiol.* **2010**, *8*, S7–S16.

(3) Lescar, J.; Luo, D.; Xu, T.; Sampath, A.; Lim, S. P.; Canard, B.; Vasudevan, S. G. *Antiviral Res.* **2008**, *80*, 94–101.

(4) Yusof, R.; Clum, S.; Wetzel, M.; Murthy, H. M.; Padmanabhan, R. *J. Biol. Chem.* **2000**, *275*, 9963–9969.

(5) Leung, D.; Schroder, K.; White, H.; Fang, N. X.; Stoermer, M. J.; Abbenante, G.; Martin, J. L.; Young, P. R.; Fairlie, D. P. *J. Biol. Chem.* **2001**, *276*, 45762–45771.

(6) Erbel, P.; Schiering, N.; D'Arcy, A.; Renatus, M.; Kroemer, M.; Lim, S. P.; Yin, Z.; Keller, T. H.; Vasudevan, S. G.; Hommel, U. *Nat. Struct. Mol. Biol.* **2006**, *13*, 372–373.

(7) Chandramouli, S.; Joseph, J. S.; Daudenarde, S.; Gatchalian, J.; Cornillez-Ty, C.; Kuhn, P. *J. Virol.* **2009**, *84*, 3059–3067.

(8) Wu, P. S. C.; Ozawa, K.; Lim, S. P.; Vasudevan, S.; Dixon, N. E.; Otting, G. *Angew. Chem., Int. Ed.* **2007**, *46*, 3356–3358.

(9) Wu, C. F.; Wang, S. H.; Sun, C. M.; Hu, S. T.; Syu, W. J. *J. Virol. Method.* **2003**, *114*, 45–54.

(10) Niyomrattanakit, P.; Winoyanuwattikun, P.; Chanprapaph, S.; Angsuthanasombat, C.; Panyim, S.; Katzenmeier, G. *J. Virol.* **2004**, *78*, 13708–13716.

(11) Phong, W. Y.; Moreland, N. J.; Lim, S. P.; Wen, D.; Paradkar, P. N.; Vasudevan, S. G. *Biosci. Rep.* **2011**, *31*, 399–409.

(12) Aleshin, A. E.; Shiryaev, S. A.; Strongin, A. Y.; Liddington, R. C. *Protein Sci.* **2007**, *16*, 795–806.

(13) Luo, D.; Xu, T.; Hunke, C.; Grüber, G.; Vasudevan, S. G.; Lescar, J. *J. Virol.* **2008**, *82*, 173–183.

(14) Robin, G.; Chappell, K.; Stoermer, M. J.; Hu, S.; Young, P. R.; Fairlie, D. P.; Martin, J. L. *J. Mol. Biol.* **2009**, *385*, 1568–1577.

(15) Radichev, I.; Shiryaev, S. A.; Aleshin, A. E.; Ratnikov, B. I.; Smith, J. W.; Liddington, R. C.; Strongin, A. Y. *J. Gen. Virol.* **2008**, *89*, 636–641.

(16) Su, X. C.; Ozawa, K.; Qi, R.; Vasudevan, S. G.; Lim, S. P.; Otting, G. *PLoS Neglected Trop. Dis.* **2009**, *3*, e561.

(17) Melino, S.; Fucito, S.; Campagna, A.; Wrubl, F.; Gamarnik, A.; Cicero, D. O.; Paci, M. *FEBS J.* **2006**, *273*, 3650–3662.

(18) Bodenreider, C.; et al. *Anal. Biochem.* **2009**, *395*, 195–204.

(19) Steuer, C.; Gege, C.; Fischl, W.; Heinonen, K. H.; Bartenschlager, R.; Klein, C. D. *Bioorg. Med. Chem.* **2001**, *29*, 4067–4074.

(20) Wichapong, K.; Pianwanit, S.; Sippl, W.; Kokpl, S. *J. Mol. Recognit.* **2009**, *23*, 283–300.

(21) Knehans, T.; Schüller, A.; Doan, D. N.; Nacro, K.; Hill, J.; Güntert, P.; Madhusudhan, M. S.; Weil, T.; Vasudevan, S. G. *J. Comput. Aided Mol. Des.* **2011**, *25*, 263–274.

(22) Schüller, A.; Yin, Z.; Chia, C. S. B.; Doan, D. N.; Kim, H. K.; Shang, L.; Loh, T. P.; Hill, J.; Vasudevan, S. G. *Antiviral Res.* **2011**, *92*, 96–101.

(23) Tomlinson, S. M.; Malmstrom, R. D.; Russo, A.; Mueller, N.; Pang, Y. P.; Watowich, S. J. *Antiviral Res.* **2010**, *82*, 110–114.

(24) Tambunan, U. S. F.; Alamudi, S. *Bioinformation* **2010**, *5*, 250–254.

(25) Frimayanti, N.; Chee, C. F.; Zain, S. M.; Rahman, N. A. *Int. J. Mol. Sci.* **2011**, *12*, 1089–1100.

(26) Satpathy, R.; Satpathy, G. R.; Rout, P. R. *Biotechnol. Bioinf. Bioeng.* **2011**, *1*, 179–182.

(27) Ghanesh, V. K.; Muller, N.; Judge, K.; Luan, C. H.; Padmanabhan, R.; Murthy, K. H. M. *Bioorg. Med. Chem.* **2005**, *13*, 257–264.

(28) Yin, Z.; Patel, S. J.; Wang, W. L.; Chan, W. L.; Rao, K. R. R.; Wang, G.; Ngew, X.; Patel, V.; Beer, D.; Knox, J. E.; Ma, N. L.; Ehrhardt, C.; Lim, S. P.; Vasudevan, S. G.; Keller, T. H. *Bioorg. Med. Chem. Lett.* **2006**, *16*, 40–43.

(29) Kiat, T. S.; Pippen, R.; Yusof, R.; Ibrahim, H.; Khalid, N.; Rahman, N. A. *Bioorg. Med. Chem. Lett.* **2006**, *16*, 3337–3340.

(30) Yin, Z.; Patel, S. J.; Wang, W. L.; Wang, G.; Chan, W. L.; Rao, K. R. R.; Alam, J.; Jeyaraj, D. A.; Ngew, X.; Patel, V.; Beer, D.; Lim, S. P.; Vasudevan, S. G.; Keller, T. H. *Bioorg. Med. Chem. Lett.* **2006**, *16*, 36–39.

(31) Yang, C. C.; Hsieh, Y. C.; Lee, S. J.; Wu, S. H.; Liao, C. L.; Tsao, C. H.; Chao, Y. S.; Chern, J. H.; Wu, C. P.; Yueh, A. *Antimicrob. Agents Chemother.* **2011**, *55*, 229–238.

(32) Cregar-Hernandez, L.; Jiao, G. S.; Johnson, A. T.; Lehrer, A. T.; Wong, T. A.; Margosiak, S. A. *Antiviral Chem. Chemother.* **2011**, *21*, 209–217.

(33) Arakaki, T. L.; Fang, N. X.; Fairlie, D. P.; Young, P. R.; Martin, J. L. *Protein Expression Purif.* **2002**, *25*, 241–247.

(34) Ekonomiuk, D.; Su, X. C.; Ozawa, K.; Bodenreider, C.; Lim, S. P.; Otting, G.; Huang, D.; Caflisch, A. *J. Med. Chem.* **2009**, *52*, 4860–4868.

(35) Su, X. C.; Ozawa, K.; Yagi, H.; Lim, S. P.; Wen, D.; Ekonomiuk, D.; Huang, D.; Keller, T. H.; Sonntag, S.; Caflisch, A.; Vasudevan, S. G.; Otting, G. *FEBS J.* **2009**, *276*, 4244–4255.

(36) Graham, B.; Loh, C. T.; Swarbrick, J. D.; Ung, P.; Shin, J.; Yagi, H.; Jia, X.; Chhabra, S.; Pintacuda, G.; Huber, T.; Otting, G. *Bioconjugate Chem.* **2011**, *22*, 2118–2125.

(37) Wu, P. S. C.; Ozawa, K.; Jergic, S.; Su, X. C.; Dixon, N. E.; Otting, G. *J. Biomol. NMR* **2006**, *34*, 13–21.

(38) Jia, X.; Ozawa, K.; Loscha, K.; Otting, G. *J. Biomol. NMR* **2009**, *44*, 59–67.

(39) Su, X. C.; Loh, C. T.; Qi, R.; Otting, G. *J. Biomol. NMR* **2011**, *50*, 35–42.

(40) Su, X. C.; Liang, H.; Loscha, K. V.; Otting, G. *J. Am. Chem. Soc.* **2009**, *131*, 10352–10353.

(41) Yagi, H.; Loscha, K. V.; Su, X. C.; Stanton-Cook, M.; Huber, T.; Otting, G. *J. Biomol. NMR* **2010**, *47*, 143–153.

(42) Jia, X.; Yagi, H.; Su, X. C.; Stanton-Cook, M.; Huber, T.; Otting, G. *J. Biomol. NMR* **2011**, *50*, 411–420.

(43) Chase, T.; Shaw, E. *Biochem. Biophys. Res. Commun.* **1967**, *29*, 508–514.
(44) Scheiner, C. J.; Quigley, J. P. *Anal. Biochem.* **1982**, *122*, 58–69.
(45) Bai, Y.; Milne, J. S.; Mayne, L.; Englander, S. W. *Proteins* **1993**, *17*, 75–86.
(46) Falgout, B.; Pethel, M.; Zhang, Y. M.; Lai, C. J. *J. Virol.* **1991**, *65*, 2467–2475.
(47) Li, J.; Lim, S. P.; Beer, D.; Patel, V.; Wen, D.; Tumanut, C.; Tully, D. C.; Williams, J. A.; Jiricek, J.; Priestle, J. P.; Harris, J. L.; Vasudevan, S. G. *J. Biol. Chem.* **2005**, *280*, 28766–28774.
(48) Khumthong, R.; Angsuthanasombat, C.; Panyim, S.; Katzenmeier, G *J. Biochem. Mol. Biol.* **2002**, *35*, 206–212.
(49) Barry, C. D.; North, A. C. T.; Glasel, J. A.; Williams, R. J. P.; Xavier, A. V. *Nature* **1971**, *232*, 236–245.
(50) Lee, L.; Sykes, B. D. *Biochemistry* **1983**, *22*, 4366–4373.
(51) Bertini, I.; Luchinat, C. *NMR of Paramagnetic Molecules in Biological Systems*; Benjamin-Cummings Publishing Company: San Francisco, 1986.
(52) Otting, G. *J. Biomol. NMR* **2008**, *42*, 1–9.
(53) Pintacuda, G.; Keniry, M. A.; Huber, T.; Park, A. Y.; Dixon, N. E.; Otting, G. *J. Am. Chem. Soc.* **2004**, *126*, 2963–2970.
(54) John, M.; Schmitz, C.; Park, A. Y.; Dixon, N. E.; Huber, T.; Otting, G. *J. Am. Chem. Soc.* **2007**, *129*, 13749–13757.
(55) Pintacuda, G.; Park, A. Y.; Keniry, M. A.; Dixon, N. E.; Otting, G. *J. Am. Chem. Soc.* **2006**, *128*, 3696–3702.
(56) Keizers, P. H.; Mersinli, B.; Reinle, W.; Donauer, J.; Hiruma, Y.; Hannemann, F.; Overhand, M.; Bernhardt, R.; Ubbink, M. *Biochemistry* **2010**, *49*, 6846–6855.
(57) Clore, G. M.; Iwahara, J. *Chem. Rev.* **2009**, *109*, 4108–4139.
(58) Su, X. C.; Otting, G. *J. Biomol. NMR* **2010**, *46*, 101–112.
(59) John, M.; Pintacuda, G.; Park, A. Y.; Dixon, N. E.; Otting, G. *J. Am. Chem. Soc.* **2006**, *128*, 12910–12916.

■ NOTE ADDED IN PROOF

After acceptance of the present paper, crystal structures of DENpro (serotype 3) in complex with aprotinin and a peptide inhibitor have been reported in a manuscript published ahead of print by Noble, C. G.; She, C. C.; Chao, A. T.; Shi, P. Y. *J. Virol.* **2011**, DOI: 10.1128/JVI.06225-11. The structures display a closed conformation very similar to the model of Figure 1B. A detailed comparison will have to await the release of the coordinates.